Research Article GU J Sci 38(4): 2079-2105 (2025) DOI: 10.35378/gujs.1593112

Gazi University

Journal of Science

http://dergipark.org.tr/gujs

Analytical and Numerical Investigation of Stress Distribution in Hydraulic Autofrettage Process

Dogan BARAN*, Osman BICAN, Yahya DOGU

Kırıkkale University, Faculty of Engineering and Natural Sciences, Department of Mechanical Engineering,71450, Kırıkkale, Türkiye

Highlights

- This paper focuses on investigation of stress distribution in the hydraulic autofrettage process.
- Hydraulic autofrettage process forms residual stresses to increase the fatigue life of barrel.
- The autofrettaged barrel has a higher-pressure carrying capacity.
- This study provides a comprehensive analysis of a wide range of parameters.

Article Info

Received:28 Nov 2024
Accepted: 11 Aug 2025

Keywords

Hydraulic autofrettage
Residual stress
Finite element analysis (FEA)
Barrel

Abstract

This study represents comprehensive investigations of the stress distribution for a heavy-weapon-barrel in hydraulic-autofrettage process by means of analytical and numerical methods. Analytical equations are employed to calculate elastic-plastic junction radius and optimum autofrettage-pressure. Stress distributions are calculated with certain equations specific to each stage of loading, unloading and working-pressure application. In both analytical and numerical model, bilinear-kinematic-hardening material model, plane-strain model, and Von Mises-yield-criteria are used. The investigation matrix includes a wide range of four main parameters: barrel diameter, yield strength of barrel material, autofrettage- pressure and working-pressure. The effects of these parameters on autofrettage process are presented in a comparative manner. There is a 36% reduction of Von Mises stress for autofrettaged barrel under working pressure. With increasing barrel diameter, the maximum Von Mises stress parabolically increases and its location moves to the barrel inner radius when working pressure is applied. Radius of elastic-plastic junction is directed towards the inner radius with increasing yield strength.

1. INTRODUCTION

The autofrettage process has been applied to high pressure heavy weapon barrels which are subjected to cyclic and variable loads. During each firing, the barrel undergoes high levels of loading and thermal stress, and fatigue can occur due to the dynamic and variable stress cycles [1,2].

Autofrettage process forms residual stresses to increase the pressure carrying capacity and fatigue life of thick-walled cylinders. These residual stresses developed in the cylinder material neutralize some of the stresses during working pressure and increase the pressure carrying capacity of pressure vessels.

In practice, there are two types of autofrettage process for heavy weapon barrels hydraulic and swage autofrettage. In the hydraulic autofrettage process, which is the focus in this study, the barrel is filled with a pressurized hydraulic fluid. The fluid pressure exceeds the working pressure and is high enough to form a plastic deformation at the barrel thickness. In the hydraulic autofrettage process, the pressure is gradually increased to the defined autofrettage pressure, maintained for a short period of time, and then gradually released. These stages are called loading and unloading stages. The third stage can be attributed to the working pressure application.

When the autofrettage pressure is released, a permanent residual compressive stress at the inner radius of the barrel forms while a residual tensile stress at the outer radius occurs. This residual compressive stress

*Corresponding author, e-mail: 198858002@kku.edu.tr

counteracts the secondary tensile stress when working pressure is applied. Thus, the autofrettage process improves the pressure carrying capacity and the fatigue life of the barrel.

The autofrettage process involves complex physics of plastic deformation and multiple biaxial stresses. The hydraulic autofrettage process is affected by many parameters such as autofrettage pressure, pressurization cycle, barrel material properties and barrel dimensions. Thus, many studies have been appearing in literature due to considerable enhancement results of autofrettage process especially in defense industry.

Huang [3] developed an autofrettage model that incorporates strain hardening and the Bauschinger effect, concluding that a lower Bauschinger effect factor facilitates reverse yielding under compression and significantly alters the residual stress distribution. Lee et al. [4] compared the strain hardening model with the elastic-perfectly plastic model for autofrettaged compound cylinders, demonstrating that the Bauschinger effect leads to lower compressive residual stresses in the strain hardening model. Ayob et al. [5] conducted a numerical study using ABAQUS to evaluate the autofrettage process in thick-walled cylinders and found that the autofrettage process enhances the maximum allowable internal pressure; furthermore, the optimum autofrettage pressure minimizes the equivalent stress under operating conditions, particularly at the elastic–plastic junction. Similarly, Shim et al. [6] utilized the KENDALL model alongside experimental Bauschinger effect data to assess residual stresses in SNMC 8 steel, showing that consideration of the Bauschinger effect reduces residual stresses at the inner diameter, while increasing autofrettage pressure amplifies hoop residual stresses at the bore. Babu and Balaji [7] numerically assessed the impact of autofrettage on a cylinder and reported that applying a 200 MPa autofrettage pressure resulted in a 15.7% reduction in maximum equivalent stress under a 180 MPa working pressure. Rupali and Mondal [8], employing the von Mises yield criterion, examined residual stress distributions in a spherical pressure vessel and concluded that autofrettage beyond 70% induces an undesirable increase in tensile hoop stress at the outer surface. They also highlighted the strong influence of the Bauschinger effect, which significantly reduces hoop stresses near the bore. Jabur et al. [9] performed a numerical investigation using ABAQUS and the von Mises yield criterion to analyze the effects of autofrettage on radial, hoop, and Von Mises stresses in a thick-walled cylinder. Their findings revealed that autofrettage reduces and redistributes maximum equivalent stresses from the inner surface toward the wall thickness, with stress reductions ranging from 3.6% to 19.2% depending on the applied autofrettage pressure. In an experimental study, Jain et al. [10] measured the residual hoop stress in a 6082T6 aluminum alloy common rail injector subjected to hydraulic autofrettage and found an 18.75% reduction in maximum von Mises stress, indicating a reduced risk of fatigue failure. Çandar and Filiz [11] analyzed the hydraulic autofrettage of a high-pressure cylinder used in a waterjet intensifier pump, reporting a 24.67% decrease in maximum von Mises stress—from 821.7 MPa in the non-autofrettaged case to 618.93 MPa under working conditions. In another study, Huang and Tang [12] proposed an autofrettage model based on kinematic hardening and the Bauschinger effect, determining an optimal autofrettage pressure of 817 MPa. Using the stress-life method, they demonstrated that autofrettage increases the minimum fatigue life of high-pressure cylinders by a factor of 15. Repplinger et al. [13] performed finite element analyses in ANSYS, following the FKM guideline, to identify the critical crack area and determine the optimal autofrettage pressure (2500 bar) for an aluminum valve body in a hydrogen fuel cell. The results, validated through hydraulic fatigue testing, showed that despite limited crack initiation at the valve stem, the component met the design requirement of 150,000 cycles without failure. Similarly, Li et al. [14] developed a new bursting pressure formulation for ultra-high-pressure (UHP) vessels and confirmed that autofrettage significantly improves fatigue life compared to conventional designs, enabling accurate fatigue life prediction. Finally, Hu and Parker [15] investigated the stress–strain response on the inner surface of fracture pump forged end blocks (FEBs) using a user-defined FEA model (USERMAT) that incorporates actual material behavior and the Bauschinger effect. Comparison with the bilinear kinematic hardening (BKIN) model revealed that while both models produced similar stress levels during loading at 500 MPa autofrettage pressure, notable differences emerged during unloading, with the BKIN model predicting more uniform and higher residual stresses than the USERMAT model.

This study has a comprehensive investigation of the stress distribution for a heavy weapon barrel in hydraulic autofrettage process by means of analytical and numerical methods. The stress distribution is

calculated in loading and unloading stages of hydraulic autofrettage process and working pressure application.

In the analytical study, analytically governed equations are employed to calculate elastic-plastic junction radius and optimum autofrettage pressure. First, the stress distributions are calculated with Lame equations for the non-autofrettaged barrel under working pressure.

Stress distributions during autofrettage process are calculated with certain equations specific to loading and unloading stages and working pressure application.

In the numerical study, the FEA model for hydraulic autofrettage process is built by using ANSYS FEA software. In the FEA model and in the analytical calculations; bilinear kinematic hardening material model, plane strain model, and Von Mises yield criteria are used.

The investigation matrix includes four main parameters: barrel diameter, yield strength of barrel material, autofrettage pressure and working pressure. A wide range of parameter values are determined by considering the applications in the field. Effects of these parameters on autofrettage process are presented in a comparative manner. Thus, this study comprehensively investigates the effect of main parameters at a wide range.

2. HYDRAULIC AUTOFRETTAGE ANALYTICAL CALCULATION

In hydraulic autofrettage process, the barrel inner diameter is exposed to a controlled internal autofrettage pressure above the elastic strength limit of the barrel material to form an elastic-plastic zone in the wall thickness. The inner radius region undergoes a greater deformation than the outer radius region. The inner radius region undergoes a plastic deformation while the outer radius region deforms elastically. When the autofrettage pressure is released, the plastically deformed inner radius region prevents the outer radius region from returning its initial dimensions, thus, a permanent residual stress occurs in radially inward direction. The loads generated in radially outward direction during the firing shots are greatly reduced because of this permanent residual stress.

In following subsections, the optimum autofrettage pressure and the radius of elastic-plastic junction is calculated. These two values are important parameters for stress calculations. The autofrettage process includes autofrettage pressure loading and unloading before working pressure application. Before the calculation of the stress distributions occurring in all three autofrettage stages, the basic equations for autofrettage process for stress calculations are defined. Then, stress distributions under loading, unloading and working pressure are calculated based on the boundary conditions and assumptions.

2.1. Radius of Elastic-Plastic Junction

When hydraulic autofrettage pressure is applied, the material undergoes plastic deformation from the inner radius to the outer radius up to a certain radius. The boundary line along which the material remains in the plastic zone and passes into the elastic zone is called the radius of elastic-plastic junction (b) as shown in Figure 1. The main objective here is to minimize the level of the maximum equivalent stress at the elastic-plastic junction [11,16].

The radius of elastic-plastic junction (b) is calculated by using following equation [17]

$$b = a \times e^{\left(\frac{\sqrt{3}P_w}{2\sigma_y}\right)} \tag{1}$$

where a is the barrel inner radius, P_w is the working pressure, and σ_y is the yield strength of the barrel material.

The radius of elastic-plastic junction is used to calculate the optimum autofrettage pressure in the hydraulic autofrettage process.

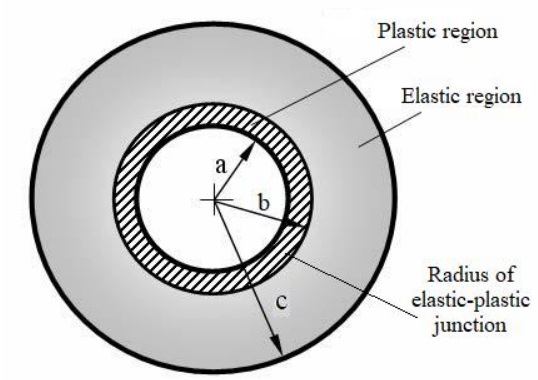


Figure 1. *Schematic view of the radius of elastic-plastic junction*

2.2. Optimum Autofrettage Pressure

In the hydraulic autofrettage process, the optimum autofrettage pressure is determined to have Von Mises equivalent stress at a minimum level on the elastic-plastic junction under the working pressure. The optimum autofrettage pressure (P_{opt}) is calculated with the following equation [11]

- $\sigma_r=\sigma_{rp}$ (at r=b)

$$P_{opt} = \frac{1}{\sqrt{3}}\left[2Aln\frac{b}{a} + (\sigma_y - A)b^2\left(\frac{1}{a^2} - \frac{1}{b^2}\right) - \sigma_y b^2\left(\frac{1}{c^2} - \frac{1}{b^2}\right)\right]. \quad (2)$$

2.3. Basic Equations for Autofrettage Process for Stress Calculations

When a thick-walled cylinder, closed at one end, is subjected to a pressure as shown in Figure 2, radial (σ_r), tangential (σ_θ) and axial (σ_z) stresses occur on the cylinder wall. These stresses are principal stresses. When a force equation is written on an infinitesimal differential element and set to zero in the radial direction, the following equations are obtained [18]

$$\Sigma F_r = 0$$

$$\sigma_r r d\theta + 2\sigma_\theta \sin\frac{d_\theta}{2} dr - \left((\sigma_r + d\sigma_r)(r + d_r)d_\theta\right) = 0 \quad (3)$$

$$\sigma_r r d\theta + 2\sigma_\theta \sin\frac{d_\theta}{2} dr - \sigma_r r d_\theta - \sigma_r d_\theta d_r - d\sigma_r r d_\theta - d\sigma_r d_\theta d_r = 0. \quad (4)$$

The term of "$d\sigma_r d_r d_\theta$" is very small and can be neglected, and assuming $\sin\frac{d_\theta}{2} \cong \frac{d_\theta}{2}$, the equation above is reduces to

$$\sigma_\theta d_r - \sigma_r d_r - r d\sigma_r = 0 \quad (5)$$

$$\sigma_r + r\frac{d\sigma_r}{d_r} - \sigma_\theta = 0. \quad (6)$$

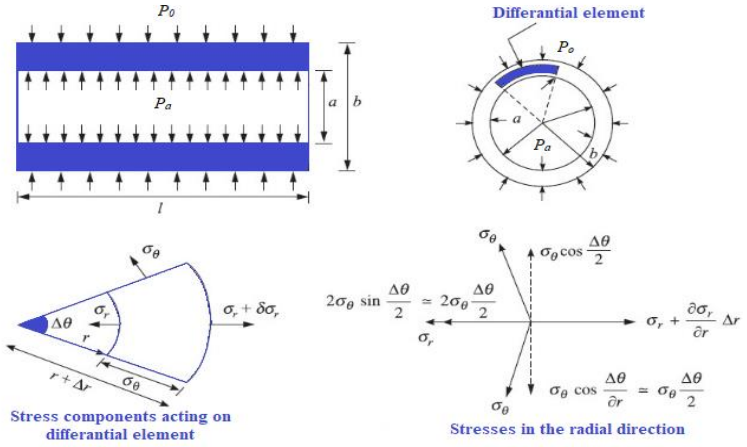


Figure 2. *Cross-sectional view of a thick-walled cylinder exposed to internal pressure*

The following equations are obtained by using both the stress-strain relationship in the elastic region and the Hooke's Law

$$\varepsilon_r = \frac{1}{E}\left(\sigma_r - \vartheta(\sigma_\theta + \sigma_z)\right)$$

$$\varepsilon_\theta = \frac{1}{E}\left(\sigma_\theta - \vartheta(\sigma_r + \sigma_z)\right)$$

$$\varepsilon_z = \frac{1}{E}\left(\sigma_z - \vartheta(\sigma_r + \sigma_\theta)\right). \tag{7}$$

During the hydraulic autofrettage process, since the barrel is fixed between the two main columns on the autofrettage machine, there is no elongation in the axial direction and the plane strain is zero (ε_z=0), thus, this fact is considered in the analytical model.

The equivalent stress-strain behavior during the autofrettage process is taken as similar to the simple compression and tensile tests of the material. The incompressible volume is assumed to be constant ($\epsilon_\theta+\epsilon_r+\epsilon_z$=0). Von Mises yield criteria is used [3,11] By using Von Mises yield criteria, stress and strain are calculated with the following equations

$$\sigma_{eq} = \sqrt{\frac{1}{2}[(\sigma_\theta - \sigma_r)^2 + (\sigma_r - \sigma_z)^2 + (\sigma_z - \sigma_\theta)^2} \tag{8}$$

$$\epsilon_{eq} = \frac{\sqrt{2}}{3}\sqrt{[(\epsilon_\theta - \epsilon_r)^2 + (\epsilon_r - \epsilon_z)^2 + (\epsilon_z - \epsilon_\theta)^2}. \tag{9}$$

For the plain strain assumption (ε_z=0), Equation (7) gives

$$\sigma_z = \frac{1}{2}(\sigma_\theta + \sigma_r). \tag{10}$$

Based on Von Mises yield criteria, when Equation (10) is substituted into Equation (8), the tangential (σ_θ) and axial stresses (σ_z) are obtained as follows

$$\sigma_\theta = \frac{2}{\sqrt{3}}\sigma_{eq} + \sigma_r \tag{11}$$

$$\sigma_z = \frac{1}{\sqrt{3}}\sigma_{eq} + \sigma_r. \tag{12}$$

The radial stress (σ_r) is obtained by using Equations (6) and (11) as follows

$$\sigma_r = \int \frac{2}{\sqrt{3}}\frac{\sigma_{eq}}{r}dr. \tag{13}$$

Equivalent strain ε_{eq} can be obtained by using plane strain and incompressible volume assumptions as follows

$$\varepsilon_\theta = \frac{u}{r} = \frac{c}{r^2} \tag{14}$$

$$\varepsilon_r = \frac{d_u}{d_r} = -\frac{c}{r^2} \tag{15}$$

where ε_θ and ε_r are the maximum and the minimum principal strains, respectively.

When Equations (14) and (15) are substituted in Equation (9), ε_{eq} is obtained as follows

$$\varepsilon_{eq} = \frac{2}{\sqrt{3}}\frac{c}{r^2} \tag{16}$$

where c is the integral constant.

2.4. Relation of Stress-Strain

In general, materials exhibit different mechanical behavior in the elastic and plastic regions. In the elastic region, when the load is released, the material returns back to its original shape. In the plastic region, when the load is applied to material beyond its elastic limit, the plastic deformation occurs. Material undergoes a permanent deformation upon removing of the load.

In this study, it is assumed that the stress-strain relationship of the barrel material is accompanied by bilinear kinematic hardening model as shown in Figure 3. The model consists of two regions: elastic (O-A) and plastic (A-B)

- In elastic region (O-A)

$$\sigma_z = \frac{1}{2}(\sigma_\theta + \sigma_r). \tag{17}$$

- In plastic region (A-B)

$$\sigma = \sigma_y + T(\varepsilon_p - \varepsilon_y) \tag{18}$$

where σ_y is the yield strength, ε_y is the yield strain, ε_p is the plastic strain, and T is the tangent modulus.

When Equation (20) is arranged

$$\sigma = A + T\varepsilon_p \tag{19}$$

where A is a constant and depends on σ_y, ε_y and T

$$A = \sigma_y - T\epsilon_y. \tag{20}$$

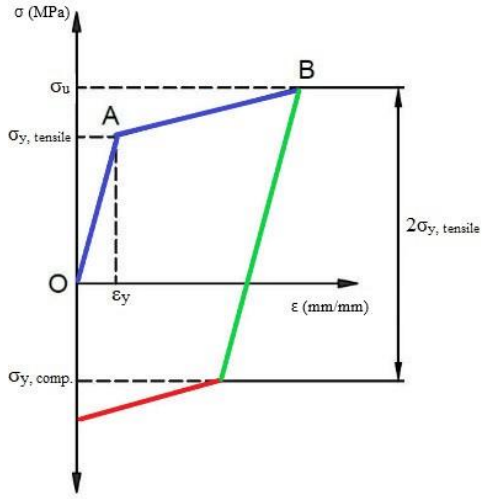


Figure 3. *Stress-strain curve based on bilinear kinematic hardening model [11]*

The Bauschinger effect is not considered in this study. The stresses developing under the working pressure are obtained by superposition of the residual stresses developing during the unloading phase and the elastic stresses developing when the working pressure is applied.

The stress equations in the elastic and plastic regions are given below

- Elastic Region (O-A)

When Equations (16) and (17) are substituted in Equation (13), Equation (21) is obtained

$$\sigma_{re} = -\frac{2}{3}\frac{E}{r^2}c_{e1} + c_{e2}. \tag{21}$$

When Equations (16), (17) and (21) are substituted in Equation (11), Equation (22) is obtained

$$\sigma_{\theta e} = \frac{2}{3}\frac{E}{r^2}c_{\theta 1} + c_{\theta 2}. \tag{22}$$

When Equations (16), (17) and (21) are substituted in Equation (12), Equation (23) is obtained

$$\sigma_{ze} = c_{e2}. \tag{23}$$

- Plastic Region (A-B)

When Equations (16) and (19) are substituted in Equation (13), Equation (24) is obtained

$$\sigma_{rp} = \frac{2}{\sqrt{3}}Alnr - \frac{2}{3}\frac{T}{r^2}c_{p1} + c_{p2}. \tag{24}$$

When Equations (16) and (19) are substituted in Equation (11), Equation (25) is obtained

$$\sigma_{\theta p} = \frac{2}{\sqrt{3}} A(1 + lnr) + \frac{2}{3}\frac{T}{r^2} c_{p1} + c_{p2}. \tag{25}$$

When Equations (16) and (19) are substituted in Equation (12), Equation (26) is obtained

$$\sigma_{zp} = \frac{1}{\sqrt{3}} A(1 + 2lnr) + c_{p2}. \tag{26}$$

When a barrel is exposed to the internal pressure of P_a (Figure 4), the boundary conditions are as follows

(1) Equivalent stresses are equal to the yield strength of the barrel material in the elastic and plastic region (at r=b)

- r=b, $\sigma_{eq,\,e}=\sigma_y$, is found as

$$c_{p1} = \frac{\sqrt{3}}{2}\frac{(\sigma_y - A)}{T} b^2. \tag{28}$$

(2) The radial stress (σ_r) in the outer radius of barrel material is equal to 0 and the radial stress in the inner radius is equal to the pressure of $-P_a$.

- r=c, $\sigma_{re}=0$, is found as

$$c_{e2} = \frac{1}{\sqrt{3}} \sigma_y \frac{b^2}{c^2}. \tag{29}$$

- r=a, $\sigma_{rp}=-P_a$, is found as

$$c_{p2} = \frac{2}{\sqrt{3}} Alna - \frac{1}{\sqrt{3}}(\sigma_y - A)\frac{b^2}{a^2} - P_a. \tag{30}$$

Based on the boundary conditions and assumptions used in the studies of Huang [3] and Çandar and Filiz [11]; and the radial (σ_r), tangential (σ_θ) and axial (σ_z) stresses developed in the elastic and plastic regions under loading, unloading and working pressure are calculated by using equations from (31) to (48).

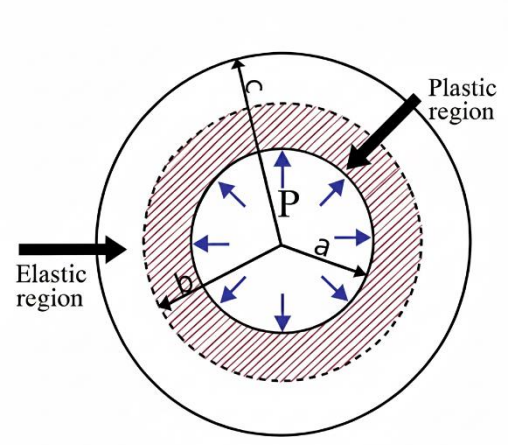


Figure 4. *Radius of elastic-plastic junction*

2.5. Stress Distribution in Loading Stage

When Equations (27) and (29) are substituted into Equations (21) to (23), Equations (31), (32) and (33) are obtained

- Elastic Region (O-A)

$$\sigma_{re} = \frac{1}{\sqrt{3}}\sigma_y b^2\left(\frac{1}{c^2}-\frac{1}{r^2}\right) \tag{31}$$

$$\sigma_{\theta e} = \frac{1}{\sqrt{3}}\sigma_y b^2\left(\frac{1}{c^2}+\frac{1}{r^2}\right) \tag{32}$$

$$\sigma_{ze} = \frac{1}{\sqrt{3}}\sigma_y \frac{b^2}{c^2}. \tag{33}$$

- Plastic Region (A-B)

When Equations (28) and (30) are substituted into Equations (24) to (26), Equations (34), (35) and (36) are obtained

$$\sigma_{rp} = \frac{1}{\sqrt{3}}\sigma_y b^2\left(\frac{1}{c^2}-\frac{1}{r^2}\right) - P_a\frac{a^2}{c^2-a^2}\left(1-\frac{c^2}{r^2}\right) - P_a \tag{34}$$

$$\sigma_{\theta p} = \frac{2}{\sqrt{3}}A\left(1+\ln\frac{r}{a}\right) + \frac{b^2}{\sqrt{3}}(\sigma_y - A)\left(\frac{1}{a^2}+\frac{1}{r^2}\right) - P_a \tag{35}$$

$$\sigma_{zp} = \frac{1}{\sqrt{3}}A + \frac{2}{\sqrt{3}}A\ln\frac{r}{a} + \frac{1}{\sqrt{3}}(\sigma_y - A)\frac{b^2}{a^2} - P_a. \tag{36}$$

2.6. Stress Distribution in Unloading Stage

When the autofrettage pressure is totally released, if the yield stress in the compression is not smaller than that of the Bauschinger effect (if there is no reverse yielding), the unloading stage exhibits elastic behavior. In this case, as Bauschinger effect is not considered, the stresses after unloading can be calculated with Lame's equations. As a result, the residual stresses in the elastic and plastic regions of the barrel material can be calculated by the following equations.

- Residual stresses in the elastic part of the gun barrel material ($b \le r \le c$)

$$\sigma_{re} = \frac{1}{\sqrt{3}}\sigma_y b^2\left(\frac{1}{c^2}-\frac{1}{r^2}\right) - P_a\frac{a^2}{c^2-a^2}\left(1-\frac{c^2}{r^2}\right) \tag{37}$$

$$\sigma_{\theta e} = \frac{1}{\sqrt{3}}\sigma_y b^2\left(\frac{1}{c^2}+\frac{1}{r^2}\right) - P_a\frac{a^2}{c^2-a^2}\left(1+\frac{c^2}{r^2}\right) \tag{38}$$

$$\sigma_{ze} = \frac{1}{\sqrt{3}}\sigma_y \frac{b^2}{c^2} - P_a\frac{a^2}{c^2-a^2}. \tag{39}$$

- Residual stresses in the plastic part of the gun barrel material ($a \le r \le b$)

$$\sigma_{rp} = \frac{2}{\sqrt{3}} A ln \frac{r}{a} + \frac{b^2}{\sqrt{3}} (\sigma_y - A) \left(\frac{1}{a^2} - \frac{1}{r^2} \right) - P_a - P_a \frac{a^2}{c^2 - a^2} \left(1 - \frac{c^2}{r^2} \right) \tag{40}$$

$$\sigma_{\theta p} = \frac{2}{\sqrt{3}} A \left(1 + ln \frac{r}{a} \right) + \frac{b^2}{\sqrt{3}} (\sigma_y - A) \left(\frac{1}{a^2} + \frac{1}{r^2} \right) - P_a - P_a \frac{a^2}{c^2 - a^2} (1 + \frac{c^2}{r^2}) \tag{41}$$

$$\sigma_{zp} = \frac{1}{\sqrt{3}} A + \frac{2}{\sqrt{3}} A ln \frac{r}{a} + \frac{1}{\sqrt{3}} (\sigma_y - A) \frac{b^2}{a^2} - P_a - P_a \frac{a^2}{c^2 - a^2}. \tag{42}$$

2.7. Stress Distribution in Working Stage

When the working pressure is applied to the inner radius, the total stress in the barrel will decrease as a result of the compressive residual stresses developing at the inner radius of the barrel. These stresses can be calculated by the following equations.

(1) Residual stresses in the elastic part of the gun barrel material under the operating pressure (b≤r≤c)

$$\sigma_{re} = \frac{1}{\sqrt{3}} \sigma_y b^2 \left(\frac{1}{c^2} - \frac{1}{r^2} \right) - P_a \frac{a^2}{c^2 - a^2} \left(1 - \frac{c^2}{r^2} \right) + P_w \frac{a^2}{c^2 - a^2} (1 - \frac{c^2}{r^2}) \tag{43}$$

$$\sigma_{\theta e} = \frac{1}{\sqrt{3}} \sigma_y b^2 \left(\frac{1}{c^2} + \frac{1}{r^2} \right) - P_a \frac{a^2}{c^2 - a^2} \left(1 + \frac{c^2}{r^2} \right) + P_w \frac{a^2}{c^2 - a^2} (1 + \frac{c^2}{r^2}) \tag{44}$$

$$\sigma_{ze} = \frac{1}{\sqrt{3}} \sigma_y \frac{b^2}{c^2} - P_a \frac{a^2}{c^2 - a^2} + P_w \frac{a^2}{c^2 - a^2}. \tag{45}$$

(2) Residual stress in the plastic part of the gun barrel material under the operating pressure (a≤r≤b)

$$\sigma_{rp} = \frac{2}{\sqrt{3}} A ln \frac{r}{a} + \frac{b^2}{\sqrt{3}} (\sigma_y - A) \left(\frac{1}{a^2} - \frac{1}{r^2} \right) - P_a - P_a \frac{a^2}{c^2 - a^2} \left(1 - \frac{c^2}{r^2} \right) + P_w \frac{a^2}{c^2 - a^2} (1 - \frac{c^2}{r^2}) \tag{46}$$

$$\sigma_{\theta p} = \frac{2}{\sqrt{3}} A \left(1 + ln \frac{r}{a} \right) + \frac{b^2}{\sqrt{3}} (\sigma_y - A) \left(\frac{1}{a^2} + \frac{1}{r^2} \right) - P_a - P_a \frac{a^2}{c^2 - a^2} \left(1 + \frac{c^2}{r^2} \right) + P_a \frac{a^2}{c^2 - a^2} (1 + \frac{c^2}{r^2}) \tag{47}$$

$$\sigma_{zp} = \frac{1}{\sqrt{3}} A + \frac{2}{\sqrt{3}} A ln \frac{r}{a} + \frac{1}{\sqrt{3}} (\sigma_y - A) \frac{b^2}{a^2} - P_a - P_a \frac{a^2}{c^2 - a^2} + P_w \frac{a^2}{c^2 - a^2}. \tag{48}$$

3. HYDRAULIC AUTOFRETTAGE NUMERICAL CALCULATION: FEA MODEL

The hydraulic autofrettage FEA model is built by using ANSYS FEA software to calculate the stresses developing in the barrel during hydraulic autofrettage process. Due to symmetrical configuration in terms of the planar geometry and loading conditions, a quarter section of the geometry is modeled in the 2-D coordinate system as plotted in Figure 5. In the 2-D model, the highest-pressure location of the barrel in the axial direction is considered as the reference region since this region is exposed to the highest thermal stress and firing loads during the internal ballistic cycle.

The following boundary conditions as plotted in Figure 5 are defined.

(1) Quarter sections: Frictionless support boundary conditions are applied.

(2) Outer radius: This boundary is left free to move.
(3) Inner radius: Inner radius is subject to varying pressure during hydraulic autofrettage process. In the model, three stages are considered as follows and plotted in Figure 6

- autofrettage pressure loading for 30 s
- autofrettage pressure unloading for 30 s
- working pressure application for 20 ms.

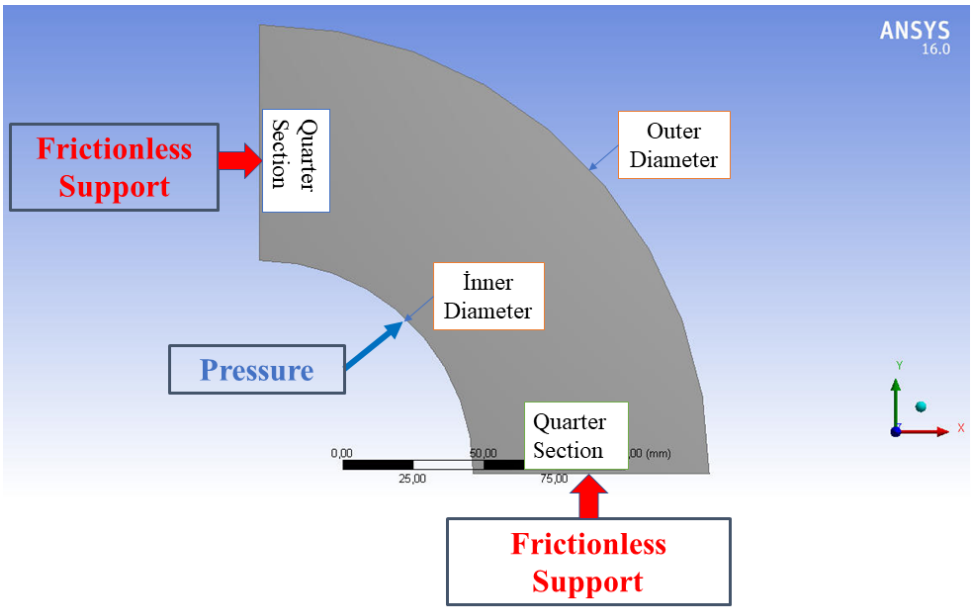


Figure 5. *Boundary conditions applied in FEA model*

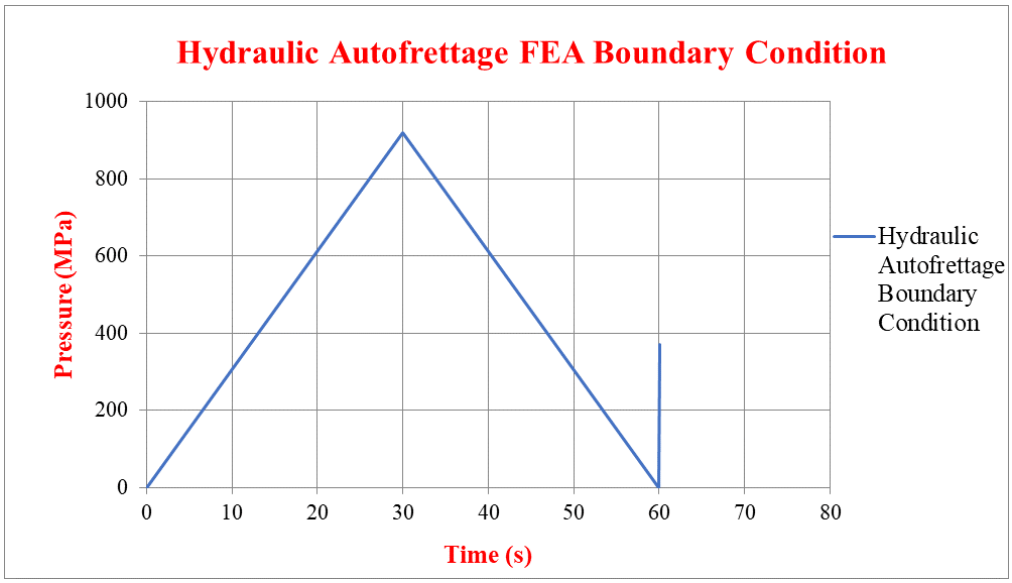


Figure 6. *Pressure variation versus time plot applied at inner radius as boundary condition*

In general, low alloy steels with high strength and toughness are used as the barrel material. In this study, the most commonly used AISI 4340 steel is selected as the barrel material and defined in the model. The chemical and mechanical properties of the AISI 4340 are listed in Tables 1 and 2 and given in Figure 7 [19]. Table 2 shows that the yield strength in the compression ($\sigma_{y,\,compressive}$) of the barrel material slightly differs from the yield strength in the tensile ($\sigma_{y,\,tensile}$). The main phenomenon behind this behavior is that the compressive residual stresses after the autofrettage process increases the fatigue life and delays the crack initiation [3,4,6,20-22]. In successive tensile and compression tests, the yield stress in the

compression reduces significantly relative to the amount of plastic strain in the previous loading condition as known as the Bauschinger effect [23].

Theoretically, when the yield stress in the tensile is equal in magnitude to that in compression, there will be no reduction in the yield strength (reverse yielding) until the ratio of outer to inner radius (k) exceeds a value of about 2.2. However, after a critical pressure threshold due to the Bauschinger effect, this phenomenon can also occur at lower ratios of k. In other words, it can take place at lower k values if yielding occurs in compression at a lower level of stress than in tension due to the Bauschinger effect [23, 24].

The Bauschinger effect is represented by the Bauschinger effect factor. This value, which is defined as the ratio of $\sigma_{y,\ compressive}/\sigma_{y,\ tensile}$, varies between 0.3-1.0 [3]. The lower this factor the lower the yield strength in the compression and Bauschinger effect factor significantly affects the residual stress distribution [6,11,23].

In practice, after autofrettage process, the material is subjected to a low temperature stress relieving process [25] and this negative effect on the residual stress is tried to be eliminated.

It is easily realized from the tensile and compression yield strength values of the material [19] that the Bauschinger effect is very small (Table 2). In analytical and numerical studies, the materials properties listed in Table 2 are used.

In the FEA, Bilinear Kinematic Hardening model is selected as the material model. Plane strain is also chosen as the material behavior.

Table 1. *Chemical composition of AISI 4340 [19]*

Fe%	Ni%	Cr%	C%	Mo%	Other%
96.6	1.8	0.8	0.4	0.25	0.1

Table 2. *Mechanical properties of AISI 4340 [19]*

Heat Treatment	$\sigma_{y,\ tensile}$ (MPa)	$\sigma_{y,\ compressive}$ (MPa)	σ_u (MPa)	E(GPa)	Tangent Modulus (MPa)	Hardness (HB)	υ
Q&T (510°C) oil	1200	1130	1270	200	1489	400	0.3

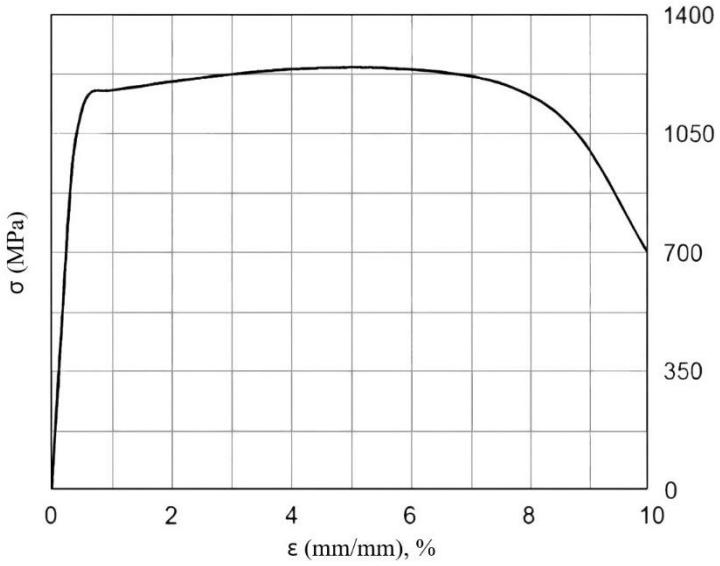


Figure 7. *Tensile stress-strain curve of AISI 4340 [19]*

For the 2-D quarter planer model, mesh independence analyses are performed for three different mesh numbers by varying minimum element size of 0.3, 0.6, and 1.2 mm which yielded number of elements between 146526, 38086, and 9591, respectively. When the results are examined for these three mesh numbers during the loading, unloading, and working stages, the calculated stress distributions are seen to be almost identical. Thus, for the sake of simplicity, 0.6 mm element size is used in all analyses. The typical mesh used in the analyses is plotted in Figure 8.

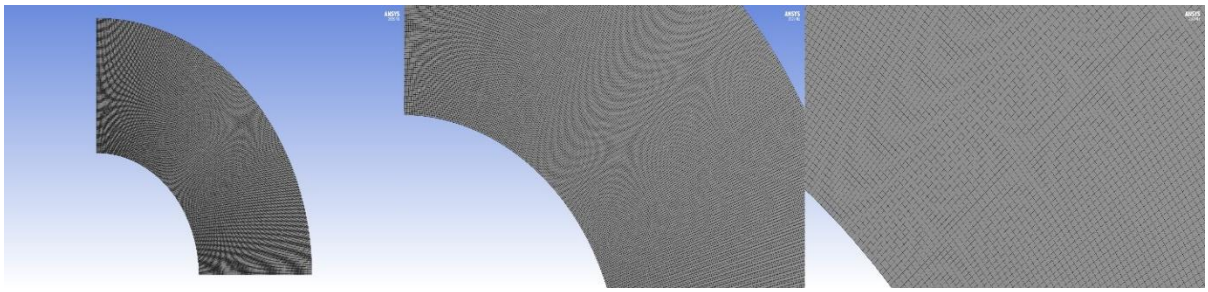


Figure 8. *Mesh structure*

The aim in this study is to parametrically investigate the stress distribution for a heavy weapon barrel in the hydraulic autofrettage process by means of analytical and numerical methods. In the investigation, four main parameters (barrel diameter, yield strength of barrel material, autofrettage pressure and working pressure) are considered. The investigation matrix and results are presented in the following section.

4. RESULTS AND DISCUSSION

In this study, the stresses forming at reference section of the autofrettaged and non-autofrettaged barrel are calculated analytically and numerically. As shown in Table 3, the investigation matrix includes four main parameters: barrel diameter, yield strength of barrel material, autofrettage pressure and working pressure. A wide range of parameter values are determined by considering the applications in the field as listed in Table 3.

A baseline case is determined in the analyses. The parameters for baseline case are notated as d_b: barrel diameter, σ_y: yield strength of barrel material, P_a: autofrettage pressure and P_w: working pressure. In Table 3, baseline case values are underlined.

The barrel diameter is varied with respect to the baseline value and four of them are considered as 0.66%, 0.77%, 0.98% and 1% of the baseline diameter.

The material yield strengths are selected as 1150 MPa, 1200 MPa and 1250 MPa, which are determined based on the lower and upper limit depending on the heat treatment process.

The total of nine values of autofrettage pressures are determined as 536.45, 600, 670, 720, 780, 840, 893.13, 954.84 and 1000 MPa. The investigation includes the working pressure as the autofrettage pressure. The maximum value of autofrettage pressure is taken as 1000 MPa, since the material fully undergo to the plastic deformation.

The working pressures used in analysis are 470 MPa, 570 MPa, and 670 MPa. The lower and upper limits of the working pressure values are determined to cover a practiced range for the considered barrel.

Table 3. *Investigation parameters and their values*

Parameters	Values								
Barrel Diameter(d/d_b)	0.66	0.77	0.98	**<u>1.00</u>**					

Yield Strength of Barrel Material (MPa)	1150	**1200**	1250						
Autofrettage Pressure (MPa)	536.45	600	670	720	780	840	893.13	**954.84**	1000
Working Pressure (MPa)	470	570	**670**						

4.1. Analysis Matrix

Based on these investigation parameters and their values, an analysis matrix in Table 4 is formed in order to systematically represent and evaluate the results in a comparative manner. The analysis matrix includes 34 cases.

A baseline case (Analysis 1) is determined by using reference barrel diameter of 150.6 mm, yield strength of barrel material of 1200 MPa, optimum autofrettage pressure of 954.8 MPa, and working pressure of 670 MPa.

Table 4. *Analysis matrix*

Analysis #	d/d_b	Yield Strength (MPa)	Autofrettage Pressure (MPa)	Working Pressure (MPa)
1	**1**	**1200**	**954.84**	**670**
2	0.98	1200	954.84	670
3	0.77	1200	954.84	670
4	0.66	1200	954.84	670
5	1	1250	954.84	670
6	**1**	**1200**	**954.84**	**670**
7	1	1150	954.84	670
8	1	1200	536.45	670
9	1	1200	600	670
10	1	1200	670	670
11	1	1200	720	670
12	1	1200	780	670
13	1	1200	840	670
14	1	1200	893.13	670
15	**1**	**1200**	**954.84**	**670**
16	1	1200	1000	670
17	1	1200	536.45	570
18	1	1200	600	570
19	1	1200	670	570
20	1	1200	720	570
21	1	1200	780	570
22	1	1200	840	570
23	1	1200	893.13	570
24	1	1200	954.84	570
25	1	1200	1000	570
26	1	1200	536.45	470
27	1	1200	600	470
28	1	1200	670	470

29	1	1200	720	470
30	1	1200	780	470
31	1	1200	840	470
32	1	1200	893.13	470
33	1	1200	954.84	470
34	1	1200	1000	470

4.2. Comparison of Analytical and Numerical Solution for Baseline Case

First of all, analytic and numeric calculation results are given and compared for the baseline case before evaluating the results for the whole analysis matrix.

In the analytical calculations, radius of elastic-plastic junction and optimum autofrettage pressure are calculated with Equations (1) and (2), respectively. The stress distribution in the loading, unloading and working pressure stages are calculated by using analytical equations from (31) to (48).

The investigation is first done for the non-autofrettaged barrel under working pressure. Figure 9 shows the stress distributions in the radial direction for the non-autofrettaged barrel under working pressure for the baseline case. The radial direction is normalized with respect to the inner and outer radius of the barrel in terms of barrel thickness percentage as r*=(r-a)/(b-a) *100. The figure has hoop, radial, axial, and Von Mises stresses obtained from both analytical and numerical calculations. It is seen that stresses obtained from the analytical and numerical calculations closely match. Only the axial stresses differ slightly and are constant at a very low value through the barrel radius. In analytical and numerical studies, axial stresses are calculated using the plane strain (ε_z=0) assumption. In reality, however, the axial strain is negligible compared to other strain values. Since the axial stress value is calculated using Equation (7) in the FEA model, the axial stress differs from the analytical result due to this small value of axial strain.

The hoop stress has its maximum value of 1067.7 MPa at inner radius while it asymptotically drops through the outer radius to the value of 394.4 MPa. The radial stress varies from -670 MPa (which is the working pressure) to 0 MPa from the inner to the outer radius. The resulting Von Mises stress at the inner radius is 1507.0 MPa which is above the yield strength of the barrel material (1200 MPa), which may adversely affect the fatigue life and the fracture mechanism and initiate the crack propagation. Therefore, autofrettage process becomes a need for barrels.

The Von Mises stress is calculated using the Lame equations. Lame equations are used to calculate stress distributions in uniform isotropic linear elastic materials. In order to make an accurate comparison with the analytical calculations, the isotropic material model is selected in the FEA model for non-autofrettaged barrel. In reality, the calculated Von Mises stress of 1507 MPa is much lower with the bilinear kinematic hardening model.

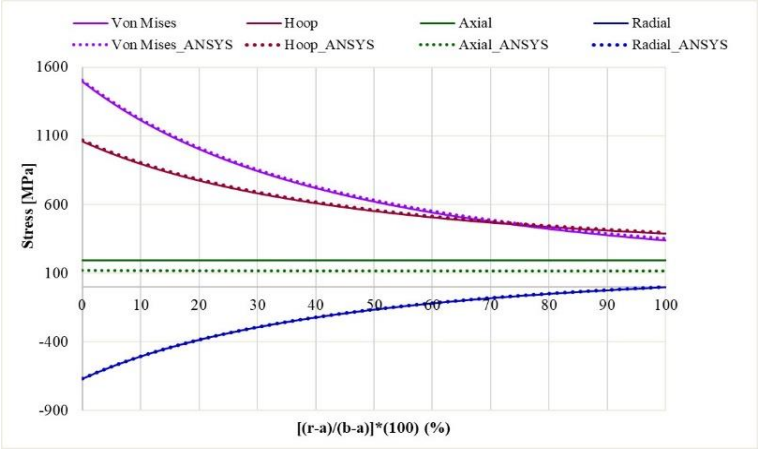


Figure 9. *Stress distribution for non-autofrettaged barrel under working pressure for baseline case*

Then, the autofrettage process is analytically and numerically modeled. In the FEA model, the autofrettage pressure is linearly increased from 0 to 954.8 MPa for 30 seconds and linearly released for upcoming 30 seconds before instantly applying the working pressure as shown in Figure 6. These three stages are continuously defined in the FEA model. The stress distributions are plotted at the end of autofrettage pressure loading stage (30s) (Figure 10a), at the end of the autofrettage pressure unloading stage (60s) (Figure10b), and under working pressure (60.02s) (Figure 10c). In addition, the stresses are compared for non-autofrettaged and autofrettaged barrel in Figure 10d. When the analytical and numerical results in Figure 10a-d are considered, they are quite similar. Again, the axial stresses differ slightly and are constant at a very low value through the barrel radius.

At the end of autofrettage pressure loading stage for the baseline case, the stress distribution is plotted in Figure 10a, and it shows that Von Mises stress is almost same at a value of 1218.8 MPa up to elastic-plastic radius (about 61% of barrel thickness), since the material in this region is subject to plastic deformation. Then, Von Mises stress almost linearly drops to 772.3 MPa. Meanwhile, the positive hoop stress values range from 453.9 MPa to 1119.8 MPa from inner radius to 61% barrel thickness, then it drops to 868.8 MPa an outer radius.

When the autofrettage pressure is totally released, as plotted in Figure 10b, the hoop stress at inner radius starts from negative values of -1073.3 MPa and almost linearly reaches a peak value of 384.1 MPa at 61% barrel thickness. Then, hoop stress slightly drops through outer radius. It should be noted that the hoop stress at the inner barrel region up to elastic-plastic radius is in the compression (-) direction which is useful to prevent the risk of crack initiation. Depending on values of axial, radial and hoop stresses, Von Mises stress has a fluctuating shape with respect to barrel thickness. Von Mises stress drops from 941.5 MPa at inner radius to 87.5 MPa at 32% barrel thickness and increases to 411.5 MPa at 61% barrel thickness then decreases to 264.7 MPa at outer radius.

At the working pressure stage, the stress distributions under the working pressure are plotted in Figure 10c. The Von Mises stress at elastic-plastic radius is 961.9 MPa for the autofrettaged barrel as seen in Figure 10c while it is 1507.0 MPa for non-autofrettaged barrel as seen in Figure 9. The autofrettage process decreased Von Mises stress by 36% under working pressure.

For comparison purposes, Figure 10d shows stress distributions for both non-autofrettaged and autofrettaged barrels under working pressure for baseline case.

Considering the stress distribution in the autofrettaged and non-autofrettaged barrel, it is seen that Von Mises stress for non-autofrettaged barrel continuously decrease with increasing radius. Meanwhile Von Mises stress for autofrettaged barrel increases up to 61% barrel thickness and then decreases. As a result, it is seen that autofrettaged barrel has a higher-pressure carrying capacity than non-autofrettaged barrel.

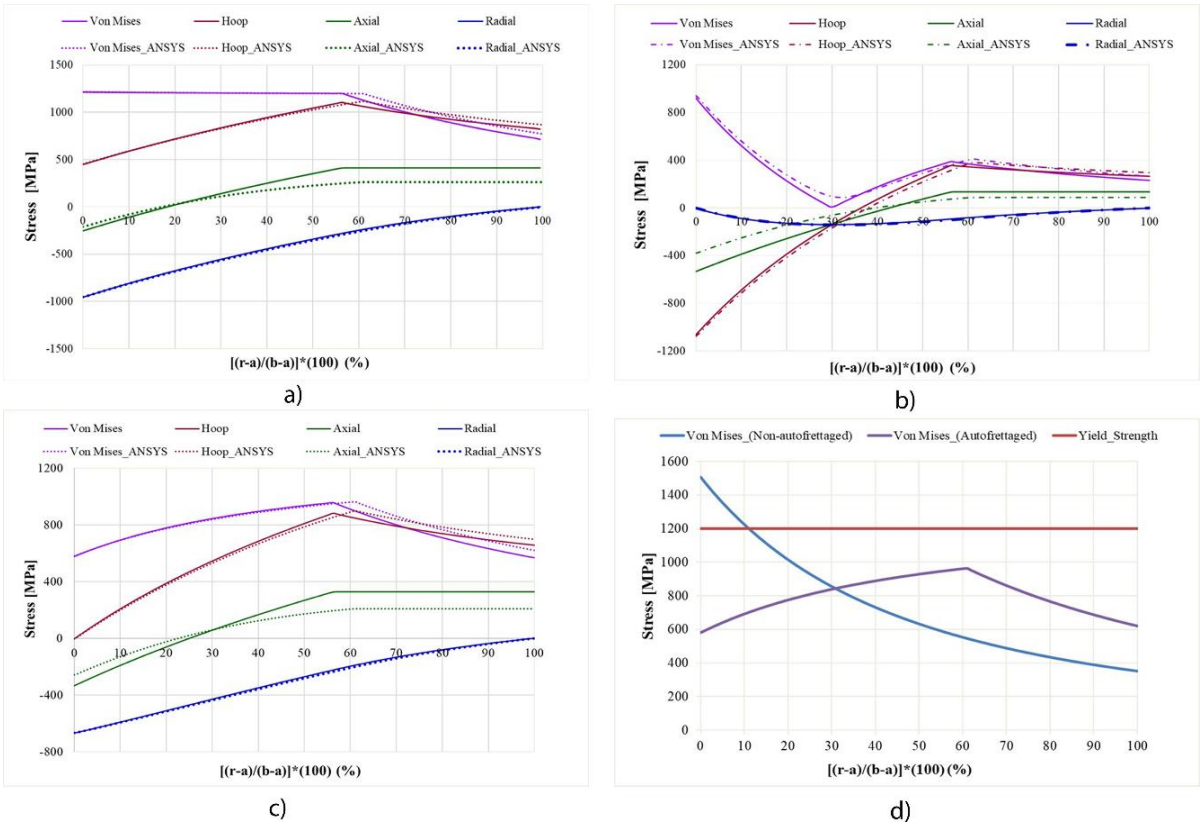


Figure 10. *Stress distribution at the end of autofrettage pressure for baseline case: a) loading b) unloading c) under working pressure d) Stress distribution comparison for non-autofrettaged and autofrettaged barrel under working pressure for baseline case*

In addition to stress distributions within the barrel thickness, Von Mises stress contours for all stages are obtained from finite element analyses and plotted for non-autofrettaged barrel and autofrettaged barrel in Figure 11a-d.

When the working pressure is applied to non-autofrettaged barrel as plotted in Figure 11a, the maximum Von Mises stress occurs at the inner radius (1507 MPa) and decreases through the outer radius (350.56 MPa).

At the end of autofrettage pressure loading, Von Mises stress has a maximum value of 1218.8 MPa at inner radius as seen in Figure 11b. This value is smaller than 1270 MPa, which is the tensile strength of barrel material. Therefore, it can be said that the optimum autofrettage pressure of 954.84 MPa is a safe value.
At the end of the unloading stage as shown Figure 11c, Von Mises stress on the inner radius is 941.53 MPa. This value is less than 1130 MPa, which is the yield strength of the material in the compression. Thus, the residual stresses obtained from autofrettage process will not be affected by the Bauschinger phenomenon and reverse yielding will not take place.

Finally, Figure 11d shows Von Mises stress contours for autofrettaged barrel under working pressure. The location of the maximum Von Mises stress occurs at 61% barrel thickness at a value of 961.96 MPa for autofrettaged barrel, while Von Mises stress has a maximum value of 1507 MPa at inner radius for non-autofrettaged barrel. There is 36% reduction of Von Mises stress for autofrettaged barrel.

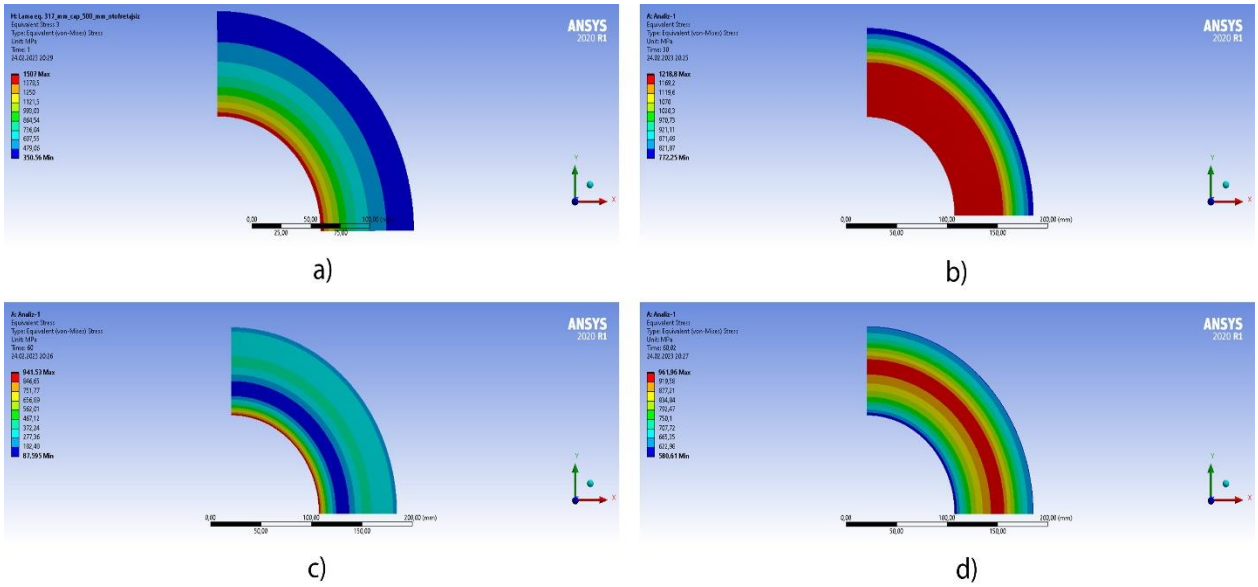


Figure 11. *Von Mises stress contours for baseline case a) for non-autofrettaged barrel under working pressure b) at the end of autofrettage pressure c) at the end of autofrettage pressure unloading d) for autofrettaged barrel under working pressure*

Specifically, Von Mises stress for autofrettaged and non-autofrettaged barrel obtained from analytical and numerical calculations under working pressure are summarized in Table 5 at certain locations of inner radius, radius of elastic-plastic junction and outer radius. As summary, autofrettage process increases pressure carrying capacity of the barrel and analytical and numerical results are compatible.

Table 5. *Comparison of analytical and numerical results in terms of Von Mises stress for autofrettaged and non-autofrettaged barrel under working pressure*

	Non-autofrettaged $\sigma_{numerical}$, (MPa)	Autofrettaged	
		$\sigma_{analytic}$, (MPa)	$\sigma_{numerical}$, (MPa)
ID	1507	576.89	580.62
Radius of elastic-plastic junction	-	957.75	961.96
OD	350.57	568.56	619.47

The results of the present study are compared with relevant literature in Table 6. When evaluating the data in the table, it should be kept in mind that the geometry, material properties, and boundary conditions are different for the referenced studies. The comparison clearly demonstrates that the reduction in maximum Von Mises stress ranges between 15.72-36%. Another fact seen on the table is that the reduction in maximum Von Mises stress increases with the applied autofrettage pressure in general.

Table 6. *Comparison between the results obtained in the present study and existing literature*

	Autofrettage Pressure (MPa)	Working Pressure (MPa)	Von Mises Stress (MPa)		Reduction of Von Mises Stress (%)
			Non-autofrettaged	Autofrettaged	
Babu and Balaji [7]	200	180	246.59	207.83	15.72
Jabur et al. [9]	130	90	290	238.79	17.65

Jain et al. [10]	202.88	150	332.31	270	18.75
Çandar and Filiz [11]	936.26	410	821.7	618.93	24.67
Present study.	954.84	670	1507	954.84	36

4.3. Diametrical Expansion

In addition to stress distribution, diametrical expansions are also calculated at the end of each stage of loading, unloading and working pressure for baseline case. The expansion at inner and outer diameter are calculated at the end of autofrettage pressure loading as 1.1216 mm and 0.62784 mm, respectively. When the autofrettage pressure is released the inner and outer diameter expansions, which are the deformations due to elastic recovery, become 0.44977 mm and 0.21499 mm, respectively. When the working pressure is applied the inner and outer diameter expansions are 0.9196 mm and 0.50343 mm, respectively. Furthermore, the inner and outer diameter expansions for non-autofrettaged barrel are calculated under working pressure as are 0.46564 mm and 0.2847 mm, respectively. In Figure (12), it is seen that, for working pressure stage, the diametrical expansions non-autofrettaged barrel are less than autofrettaged barrel.

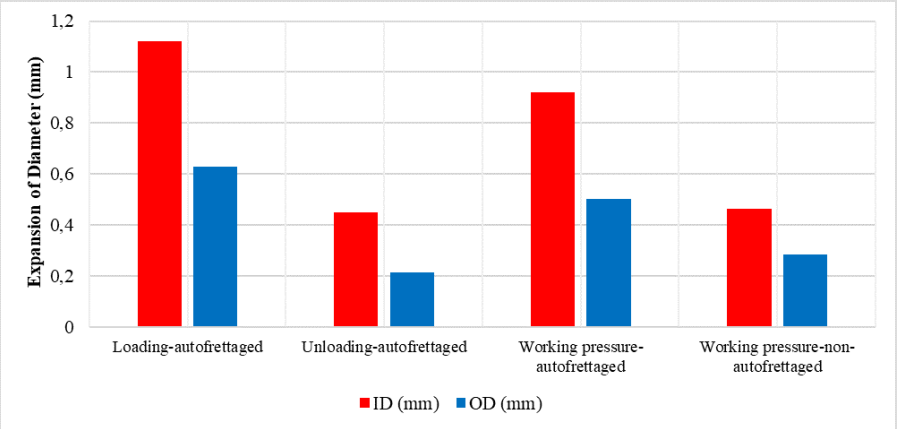


Figure 12. *Diametrical expansions at the end of each autofrettage stage for baseline case and under working pressure for non/autofrettaged barrel*

Expansion values in the inner and outer diameters with respect to the yield strength of the barrel material are also plotted in Figure 13. In conclusion, the higher yield strength, the higher resistance of the barrel material against plastic deformation and expansion of inside and outside diameter decreases.

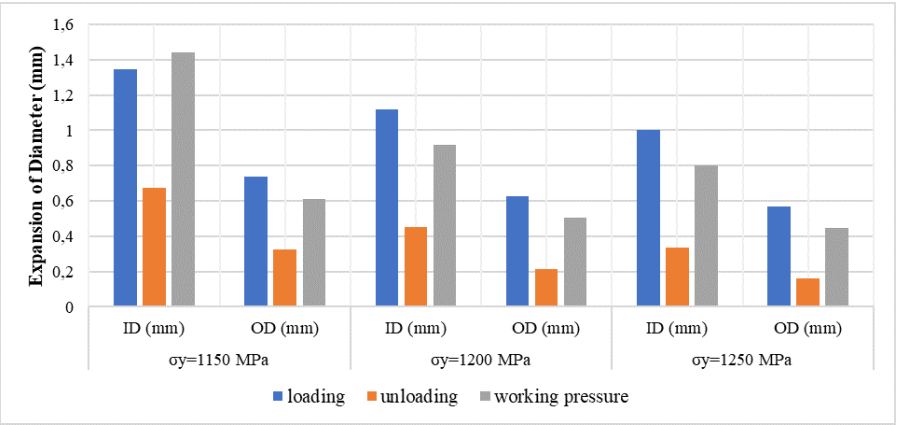


Figure 13. *Diametrical expansions with respect to the yield strength of the barrel*

4.4. Parametric Analyses

After comparing and evaluating analytical and numerical calculations, parametric analyses are only performed with FEA model.

As shown in Table 3, the investigation matrix includes four main parameters:
(1) barrel diameter,
(2) yield strength of barrel material,
(3) autofrettage pressure and
(4) working pressure.

A wide range of parameter values are determined by considering the applications in the field. By using these four investigation parameters and their values, the analyses matrix given in Table 4 is formed. There are 34 analysis cases. The analysis case 1 is determined as the baseline case by using barrel diameter of 150.6 mm, yield strength of barrel material of 1200 MPa, optimum autofrettage pressure of 954.8 MPa, and working pressure of 670 MPa. When the effect of each of four parameters is investigated, values of other parameters are kept same as in the baseline case.

At the following subsections, effect of each investigation parameters is given separately.

Effect of Barrel Diameter

Stress distribution is plotted in Figure 14a-c for various barrel diameters as listed in analysis matrix table (Tables 3 and 4). The barrel diameter is varied with respect to the baseline value and four of them are considered as 0.66%, 0.77%, 0.98% and 1% of the baseline diameter.

It is seen that the magnitude of the hoop stress developing in the compression (-) at working pressure stage reduces as the barrel diameter decreases.

The smaller barrel diameter yields the smaller Von Mises stress and Von Mises stress is directed to the barrel inner radius when working pressure is applied.

In addition, in Figure 14d, the maximum Von Mises stress and its location for various barrel diameter at working pressure stage is plotted. Increased barrel diameters almost parabolically increase the maximum Von Mises stress whose locations move through the outer radius. The maximum Von Mises stress is 879.1 MPa at 65.1 mm of barrel thickness while it is increased to 961.9 MPa at 126.5 mm of barrel thickness. Between these two investigated points, Von Mises stress increment rate with barrel diameter is determined as 1.6 MPa/mm diameter change which is quite a small number.

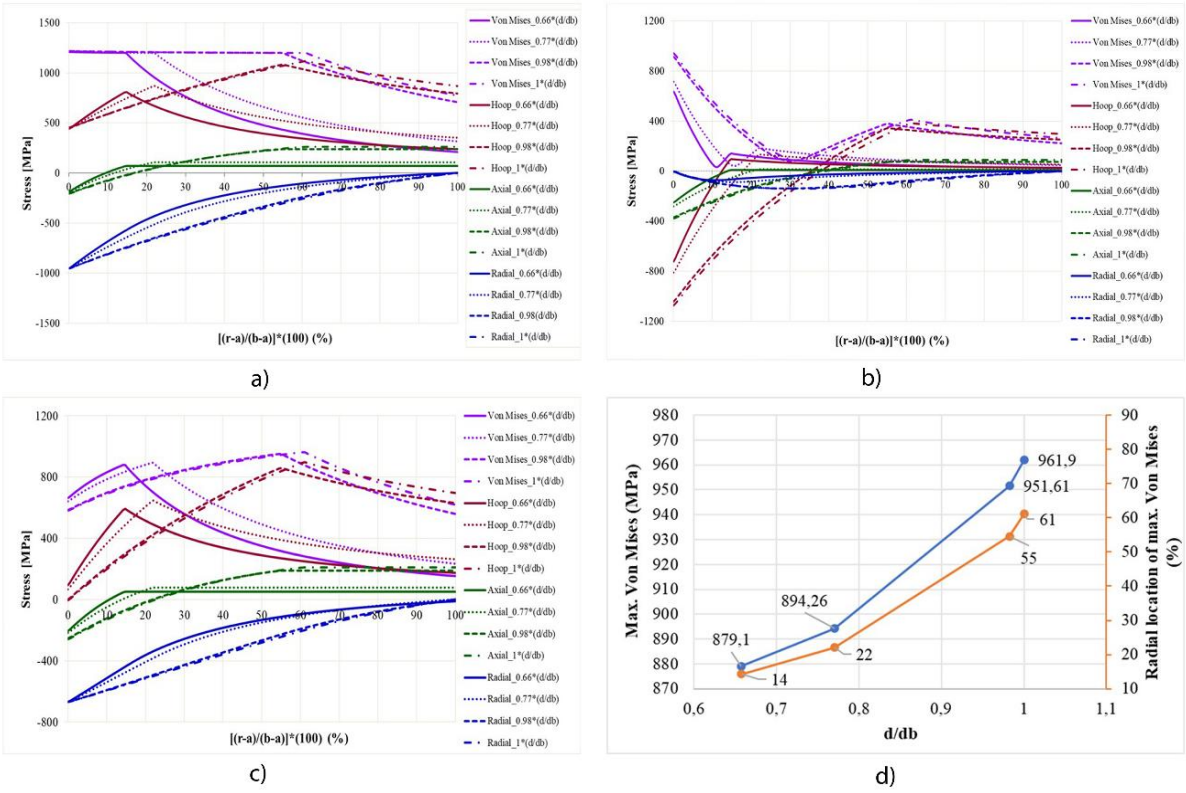


Figure 14. *Stress distribution by diameter a) Loading b) Unloading c) Working pressure d) Maximum Von Mises stress and its location for various barrel diameter at working pressure stage*

Effect of Yield Strength

In Figure 15a-c, the effect of yield strength of barrel material is plotted. The barrel materials are selected as 33NiCrMoV15, AISI 4340 and 40NiCrMoV15 steel respectively These gun barrel materials are recognized for their exceptional advanced of tensile strength, ductility and toughness. They have a high level of impact toughness due to water quenched after the austenitizing heat treatment.

Material yield strengths may vary depending on heat treatment process.

Analyses are carried out for the yield strengths of 1150 MPa, 1200 MPa and 1250 MPa, which are within the lower and upper limit values of the barrel materials.

In addition, in Figure 15d, the maximum Von Mises stress and its location for various yield strength at working pressure stage is plotted.

Radius of elastic-plastic junction is directed towards the inner radius with increasing yield strength, and located at 78%, 61%, and 50% of barrel thickness for yield strength of 1150 MPa, 1200 MPa, and 1250 MPa, respectively.

The maximum Von Mises stresses under working pressure occur at the radius of elastic-plastic junction, and are calculated as 951.39 MPa, 961.90 MPa, and 977.72 MPa for yield strength of 1150 MPa, 1200 MPa, and 1250 MPa, respectively. The increment rate of maximum Von Mises stress with yield strength is determined as 0.3 MPa/MPa yield strength change which is quite a small number.

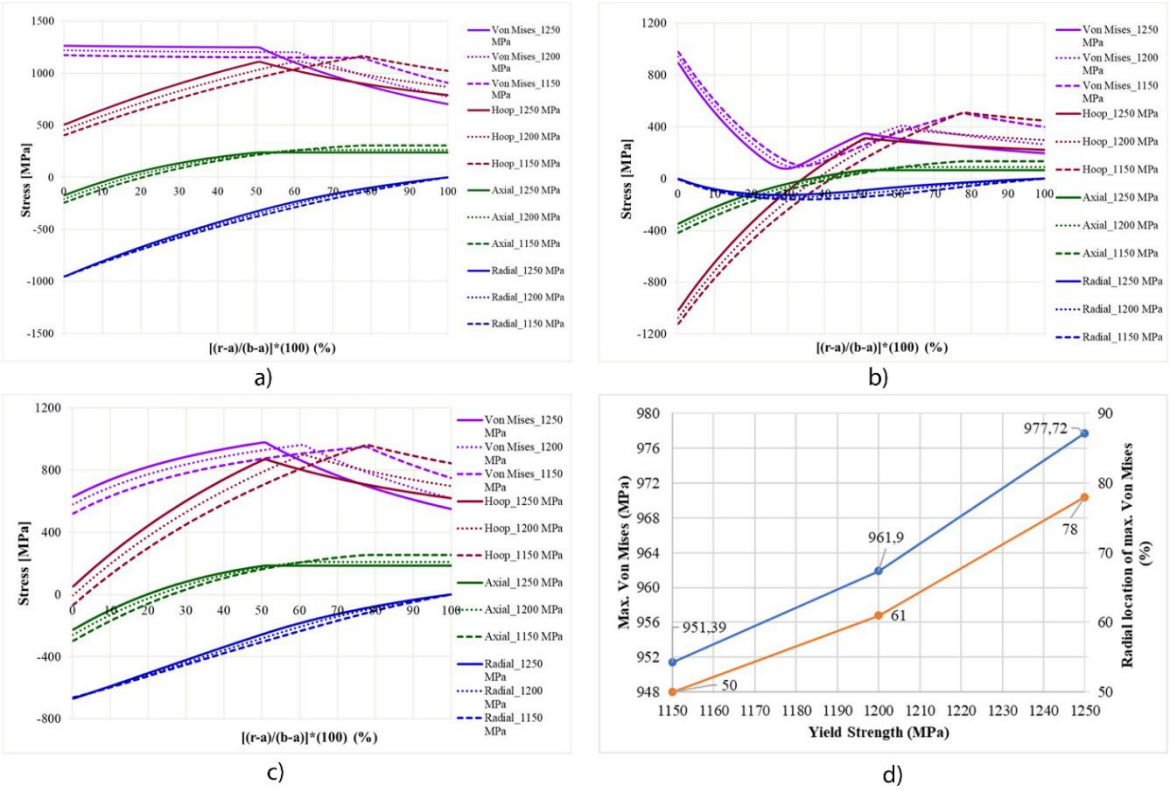


Figure 15. *Stress distribution by yield strength a) Loading b) Unloading c) Working pressure d) Maximum Von Mises and its location for various yield strength at working pressure stage*

Effect of Autofrettage Pressure

In autofrettage process, autofrettage pressure is a critical parameter. The optimum autofrettage pressure is a function of barrel inner-outer radius, mechanical properties of barrel material, and working pressure, and is calculated with Equation (2). In order to investigate the effect of autofrettage pressure, additional analyses are run for a wide range of autofrettage pressure as listed in analysis matrix, Table 4. In this investigation the baseline parameters (barrel diameter of 150.6 mm, yield strength of barrel material of 1200 MPa, working pressure of 670 MPa) are used. By considering mechanical properties of barrel material, a total of 9 different autofrettage pressures are investigated.

The minimum autofrettage pressure (P_{y1}) is defined as the starting point of yield at the barrel inner radius since the autofrettage pressure is lower than this point it is not possible to mention about any autofrettage effect. Meanwhile, the maximum autofrettage pressure (P_{y2}) can be defined as the point where the plastic deformation spreads along the barrel wall. The P_{y1} and P_{y2} pressures are calculated by the semi-empirical equations expressed in Equations (49) and (50), [26]

$$P_{y1} = \sigma_y \frac{\left(1 - \left(1 - \left({}^{1}/_{k^2}\right)\right)\right)}{\sqrt{3}} \tag{49}$$

$$P_{y2} = \sigma_y ln(k) \tag{50}$$

where k is the ratio of outer to inner radius. These equations yield P_{y1}=536.45 MPa and P_{y2}=893.13 MPa. It should be noted that optimum autofrettage pressure is calculated by using Equation (2) as 954.84 MPa which is higher than P_{y2}=893.13 MPa. Equation (50) does not include plasticity theory and material model incorporated in this work. If the autofrettage pressure is lower than 536.45 MPa, it is not possible to mention

any autofrettage effect. If the autofrettage pressure is higher than 893.13 MPa, the effectiveness of the autofrettage process is reduced gradually, that is, the pressure carrying capacity of the barrel will decrease.

The investigated 9 autofrettage pressures are 536.45, 600, 670, 720, 780, 840, 893.13, 954.84, 1000 MPa. The investigation includes the working pressure as the autofrettage pressure. The maximum value of autofrettage pressure is taken as 1000 MPa, since the material fully undergo to the plastic deformation. Since the number of investigated autofrettage pressure is high, the most critical parameter only variation of maximum Von Mises stress at the radius of elastic-plastic junction during working pressure stage is plotted with respect to autofrettage pressures in Figure 16.

Up to the autofrettage pressure value of 670 MPa which is the working pressure, Von Mises stays constant at about 1200 MPa. That is, the autofrettage pressure is lower than the working pressure, it is seen that there is no autofrettage effect. Beyond this point, Von Mises reduces to 962 MPa by increasing autofrettage pressure up to optimum autofrettage pressure of 954.84 MPa.

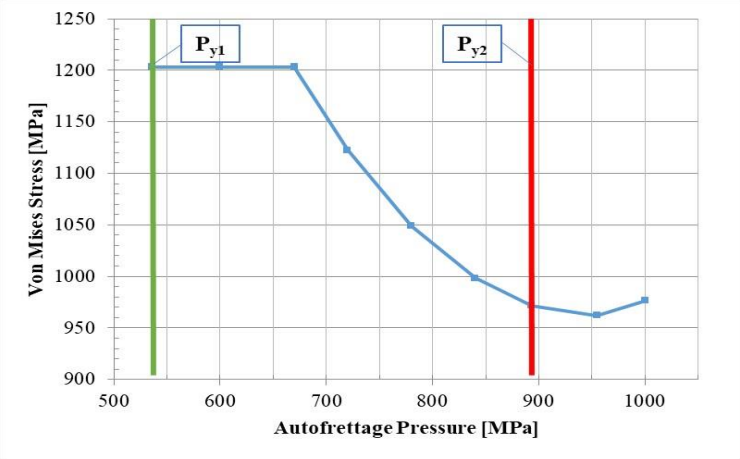


Figure 16. *Maximum Von Mises stress during working pressure stage versus autofrettage pressure for baseline case*

Effect of Working Pressure

In practice, the barrel faces different working pressures. The analyses are run for working pressures of 470 MPa, 570 MPa, and 670 MPa by considering the total of 9 autofrettage pressure values in the previous subsection. The lower and upper limits of the working pressure values are determined to cover a practiced range for the considered barrel. These analyses are also shown in analysis matrix Table 3 and 4. Since the number of analyses is high, only maximum Von Mises under working pressure stage at the radius of elastic-plastic junction is plotted with respect to autofrettage pressures and working pressures in Figure 17.

Von Mises stays constant up to an autofrettage pressure which is equal to P_{y1}=536.45 for all working pressures. For all working pressures, Von Mises stress decreases with increasing autofrettage pressure up to P_{y2}=893.13 MPa. After this value, it starts to increase.

Von Mises has similar shape for all working pressure and reduces with decreasing working pressure.

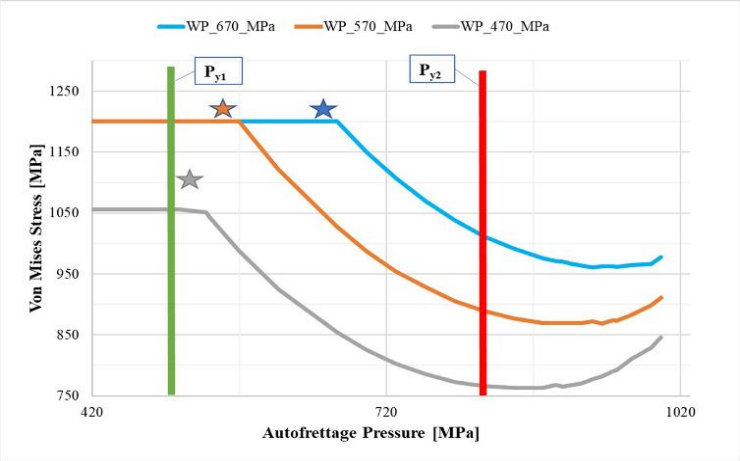


Figure 17. *Maximum Von Mises stress during working pressure stage versus autofrettage pressure and working pressure*

5. CONCLUSION

In this study, the stress distributions in hydraulic autofrettage process of a heavy weapon barrel are determined in terms of four main parameters (barrel diameter, yield strength of barrel material, autofrettage pressure and working pressure) by means of analytical and numerical methods. The study includes a large analyses matrix and considers all processes of autofrettage pressure loading-unloading and working pressure application. The main findings of the investigation are listed below.

- First, for baseline case, radius of elastic-plastic junction is calculated as 122.21 mm and the optimum autofrettage pressure as 954.84 MPa that gives the lowest value of the Von Mises under 670 MPa working pressure.

- The maximum Von Mises stress under working pressure for autofrettaged barrel is 961.96 MPa at 61% of barrel thickness, while it is 1507 MPa at inner radius for non-autofrettaged barrel. There is 36% reduction of Von Mises stress for autofrettaged barrel. Thus, the barrel with autofrettage process has a higher-pressure carrying capacity than non-autofrettaged barrel.

- With increasing barrel diameter, the maximum Von Mises stress parabolically increases and its location moves to the barrel inner radius when working pressure is applied. Von Mises stress increment rate with barrel diameter is determined as 1.6 MPa/mm diameter change which is a quite small number.

- The yield strength of barrel material is also varied between 1150 MPa and 1250 MPa. Radius of elastic-plastic junction is directed towards the inner radius with increasing yield strength while the increment rate of maximum Von Mises with yield strength is determined as 0.3 MPa/MPa yield strength change.

- The autofrettage pressure is varied between 536.45 MPa which is the yield starting point on the inner radius and 1000 MPa at which the material fully undergoes to the plastic deformation. It is found that when the autofrettage pressure is lower than the working pressure, there is no autofrettage effect. Beyond this point, Von Mises stress reduces to 962 MPa with increasing autofrettage pressure up to optimum autofrettage pressure of 954.84 MPa.

- In addition, working pressures are also varied at values of 470 MPa, 570 MPa, and 670 MPa by considering different autofrettage pressures. Von Mises stress has similar shape for all working pressure and reduces with decreasing working pressure.

Within the scope of the future work, the plan is to support this analytical and numerical work with experimental data. The expansion at inner and outer diameter can be easily measured while the residual stress measurement requires the use of some non/destructive measurement techniques such as X-ray diffraction (XRD), neutron diffraction and ultrasonic methods.

In practice, another fact to consider is the low-temperature heat treatment process of the barrel after the autofrettage. This process, typically performed slowly at a temperature between 300-375°C and cooling, reduces and eliminates dislocation accumulations caused by the Bauschinger effect. This heat treatment plays a critical role in improving the stability and reliability of the barrel. It would be more practical to develop material models that more accurately reflect the Bauschinger effect in numerical models in future studies.

CONFLICTS OF INTEREST

No conflict of interest was declared by the authors.

REFERENCES

[1] Bhatnagar, R.M., "Modelling, validation and design of autofrettage and compound cylinder", European Journal of Mechanics A/Solids, 33(2): 94-100, (2005). DOI: http://dx.doi.org/10.1016/j.euromechsol.2012.09.013

[2] Majzoobi, G.H., and Ghomi A., "Optimization of autofrettage in thick-walled cylinders", Journal of Achievements in Materials and Manufacturing Engineering, 16(1-2): 124-131, (2006).

[3] Huang, X.P., "A general autofrettage model of a thick-walled cylinder based on tensile-compressive stress-strain curve of a material", Journal of Strain Analysis for Engineering Design, 40(20): 599-607, (2005). DOI: https://doi.org/10.1243/030932405X16070

[4] Lee, E.Y., Lee, Y.S., Yang, Q.M., Kim, J.H., Cha, K.U., and Hong, S.K., "Autofrettage process analysis of a compound cylinder based on the elastic-perfectly plastic and strain hardening stress-strain curve", Journal of Mechanical Science and Technology, 23(12): 3153-3160, (2009). DOI: https://doi.org/10.1007/s12206-009-1009-9

[5] Ayob, A., Tamin, M.M., and Elbasheer, M.K., "Pressure limits of thick-walled cylinders", Proceedings of the International MultiConference of Engineers and Computer Scientists, Hong Kong, China, (2009).

[6] Shim, W.S., Kim, J.H., Lee, Y.S., Cha, K.U., and Hong, S.K., "A Study on hydraulic autofrettage of thick-walled cylinders incorporating bauschinger effect", Experimental Mechanics, 50: 621-626, (2010). DOI: https://doi.org/10.1007/s11340-009-9255-4

[7] Babu, D.D., and Balaji, T.J., "Theoretical and finite element analysis of high pressure components", IOSR Journal of Engineering, 3(2): 25-34, (2013). DOI: https://doi.org/10.9790/3021-03222534

[8] Rupali, and Mondal, S. C., "Finite element analysis for predicting residual stresses of autofrettaged spherical vessels considering bauschinger effect", International Journal of Scientific Engineering and Research (IJSER), 6(8): 912-919, (2015).

[9] Jabur, L.S., Radhi, H.I., and Mohsin, N.R., "Finite element analysis of autofrettage process of thick walled cylinders", International Journal of Mechanical Engineering and Technology, 7(5): 184-192, (2006).

[10] Jain, A., Khanwelkar, S., Saurav, S.K., Landge, A., and Yadav, U., "Design and performance of hydraulic autofrettage using universal testing machine", International Journal of Mechanical Engineering Research and Technology, 6(2): 154-157, (2016).

[11] Çandar, H., and Filiz, H., "Optimum autofrettage pressure for a high pressure cylinder of a waterjet intensifier pump", Universal Journal of Engineering Science, 5(3): 44-55, (2017). DOI: https://doi.org/10.13189/ujes.2017.050302.

[12] Huang, W., and Wencheng, T., "The optimum autofrettage and fatigue prediction based on finite-element method for high pressure cylinder", Proceedings of 3rd International Conference on Electronic Information Technology and Computer Engineering (EITCE), Xiamen, China, (2019). DOI: https://doi.org/10.1109/EITCE47263.2019.9095072

[13] Repplinger, C., Kedziora, S., Cao, T.B., Maas, S., Sellen, S., and Zürbes, A., "Numerical determination and experimental verification of the optimum autofrettage pressure for a complex aluminum high-pressure valve to foster crack closure", Fatigue and Fracture of Engineering Materials and Structures, 43: 2183-2199, (2020). DOI: https://doi.org/10.1111/ffe.13227

[14] Li, G., Deng, X., Song, H., and Zhang, B., "Research on autofrettage mechanism in ultra-high pressure thick-walled vessel", Proceedings of the 7th International Conference on Computer-Aided Design, Manufacturing, Modeling and Simulation (CDMMS 2020), Busan, South Korea, (2020). https://doi.org/10.1088/1742-6596/1802/2/022001

[15] Hu, Z., and Parker, A.P., "Numerical modeling of hydraulic autofrettage numerical modeling of hydraulic autofrettage fracture pumps based on true material model", International Journal of Mechanical and Production Engineering Research and Development, 10(5): 1-7, (2022).

[16] Ayob, A., and Elbasheer, M.K., "Optimum autofrettage pressure in thick cylinders", Jurnal Mekanikal, 24: 1-14, (2007).

[17] Zhu, R., and Yang, J., "Autofrettage of thick cylinders", International Journal of Pressure Vessels and Piping, 75: 443-446, (1998).

[18] Srivastava, A.K., and Gope, P.C., "Strength of Materials". 2nd ed., PHI Learning Private Limited, New Delhi, (2012).

[19] ASM International, "Atlas of Stress-Strain Curves" 2nd ed., Materials Park, United State of America, (2002).

[20] Trieb, F., Schedelmaier, J., and Poelzl, M., "Autofrettage - basic information and practical application on components for waterjet cutting", Proceedings of WJTA American Waterjet Conference, United State of America, Houston, Texas, United State of America, (2005).

[21] Troiano, E., Parker, A.P., Underwood, J.H., and Mossey, C., "Experimental data, numerical fit and fatigue life calculations relating to bauschinger effect in high strength armament steels", Journal of Pressure Vessel Technology, 125(3): 330-334, (2003). DOI: https://10.1115/1.1593072

[22] Perry, J., and Aboudi, J., "Elasto-plastic stresses in thick-walled cylinders", Journal of Pressure Vessel Technology, 125(3): 248-252, (2003). DOI: https://doi.org/10.1115/1.1593078

[23] Perry, J., and Perl, M., "The effects of the material's exact yield point and its plastic properties on the safe maximum pressure of gun barrels", Journal of Pressure Vessel Technology, 139(5): 051401, (2017). DOI: https://doi.org/10.1115/1.4037121

[24] Hill, R., "The Mathematical Theory of Plasticity", Oxford University Press, New York, (1950).

[25] Perl, M., Perry, J., "The beneficial influence of bauschinger effect mitigation on the barrel's safe maximum pressure", Journal of Pressure Vessel Technology, 135(2): 021404, (2013). DOI: https://doi.org/10.1115/1.4007645

[26] Ali, A.R.M., Ghosh, N.C., and Alam, T.E., "Optimum design of pressure vessel subjected to autofrettage process", International Journal of Mechanical and Mechatronics Engineering, 4(10): 1040-1045, (2010). DOI: https://doi.org/10.5281/zenodo.1083535